A MIMO architecture for SaR application

Francesco Prodi*[a], Luigi Pierno [a], Alfonso Farina (Consultant [a])
[a]Leonardo Electronics SpA, via Tiburtina km 12,4 00131 Roma, Italy

ABSTRACT

This paper propose a MIMO architecture proposed for a S-band VTS coastal radar aiming to detect, up to 10 km range, small RCS targets (<1m2) in sea state 0-5, due to rubber boats of illicit trafficking of humans and materials in SaR (Search and Rescue Maritime) Surveillance systems (*RANGER system*). The radar architecture is formed of a filled RX ULA (Uniform Linear Array) with Mr elements, and of a co-located TX ULA with Mt elements separated by $l=M_r*\lambda/2$. This basic configuration is equivalent to a uniform filled ULA with *MrMt* elements and MIMO orthogonality of TX-s waveforms is obtained by Time Domain Multiplexing of the transmitted large band FM chirp between different TX-s. The potential leakage between Doppler domain and azimuth domains put some constrains on MIMO processing. In particular it is shown how a pseudo-random law of TX array scanning may mitigate this leakage. It is then shown that a small boat may be well detected thank to fine range resolution (large bandwidth), narrow beam (large TX array aperture) and fine Doppler processing. Finally it is shown that a bi-static architecture may further improve detection performance due to both clutter cell and bi-static clutter Reflectivity reduction.

Keywords: MIMO, FMCW, TDM-MIMO, FMCW radar, SaR (Search and Rescue), STAP

1. MIMO ARCHITECTURE

MIMO architecture is composed of a filled *RX ULA* (*Uniform Linear Array*) with M_r elements, and of a co-located *TX ULA* with M_t elements separated by $M_r*\lambda/2$ (see Figure 1). Large band FM-CW pulses are sequentially transmitted with a given PRT (Pulse Repetition Time) cyclically on the TX ULA: that is TX1, TX2 up to TX M_t in the first cycle, again TX1, TX2 up to TX M_t in the second cycle, and so on for N_r cycles. This approach implements the MIMO architecture based on Time Domain Multiplexing TDM and the *Time On Target*, that is the processed frame length, is $T_o=M_t N_r*T$, where T is PRT. In standard [1] MIMO architectures, pulses could be made orthogonal to each other and transmitted simultaneously and $T_o= N_r*T$ can be made shorter, keeping the same energy on target wrt the TDM architecture. Let *B* the instantaneous Bandwidth of TX pulses and τ pulse-width. In order to maximize pulse transmitted energy $\tau \approx$PRT is assumed. Power transmitted PW by each TX is typically few Watts. Sequential transmission of TX-s limit duty-cycle of each TX to $100/M_t$.

Typically we assume the following ranges for system parameters: $M_t \in [5,20]$, $M_r \in [5,20]$ $N_r \in [4,32]$, $T \in [200,1000]$ μsec, and $B \in$ [50-200] MHz. The parameter set is obviously adapted on system specifications (i.e. radar range, target RCS, TX power..) and on hardware resources (typically M_t and M_r).

The general architecture receiver chain, typical of a FM-CW radar, for each of the M_t receivers, is reported in Figure 1. After deramping mixer the received chirp is baseband converted to a complex envelope which is indicatively the sum of beat frequencies corresponding to the range of scatterers. Range profile is then recovered, for each received pulse, by a FFT of slant range samples and also undesired harmonics of the scatterers are present in the spectrum. For each range sample the data structure is structured in the 3D complex hologram $H(M_t, M_r, N_r)$ of Figure 1.

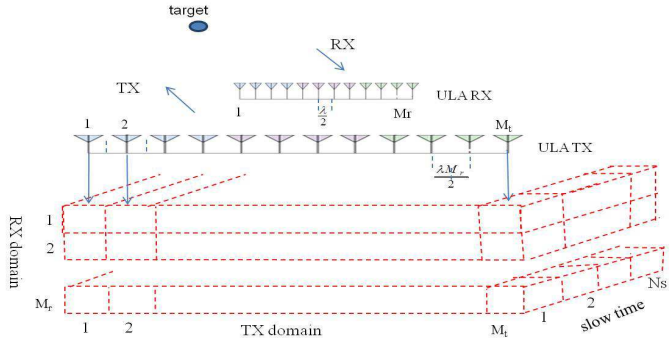

Figure 1 MIMO architecture with data structure

The four input domains together with conjugate domains and relative resolutions obtained after signal processing are reported in Table 1

input domain	output domain	processing goal
fast time	range	range resolution
RX	azimuth	azimuth resolution
TX	azimuth	azimuth resolution
slow time	Doppler	clutter cancellation

Table 1: processing domains

where *fast time* domain is the single sweep of length T sampled at range bin rate while *slow time* domain is the processing interval $T_0 = M_t N_r * T$, with sampling time M_t T in the slow-time algorithm (Par. 2.1) and T in TX staggering algorithm (Par. 2.2).

Range compression along fast time domain and Doppler processing along slow time are conventionally implemented with weighted FFT. Compression of RX-TX allows synthesis of a narrow azimuth beam, and is peculiar of MIMO processing. Also in this case azimuth compression is based on 1D FFTs along RX and TX domains. the present MIMO architecture implies only one 'big' 1D FFT along $M_r M_t$ samples of the virtual ULA elements. In this perspective the peculiar sequence of the three domains - i.e. range-azimuth-Doppler is arbitrary.

We observe that two constrains, make signal processing more complicate than a three cascaded 1D FFTs. They are:

a. range migration compensation
b. leakage between slow time and spatial-TX domains due to TDM transmission operation

Constraint a) implies, for large arrays (indicatively $M_r>5$) splitting azimuth beam-forming into two separate TX and RX compressions. It will be considered later.

Constraint b) lead to a deviation from the standard MIMO processing based of use on orthogonal waveforms (more generally: linearly independent) transmitted by different TX-s in the same frame time of length T. This fact is now explained is now described.

Referring to the standard (orthogonal waveform simultaneous Tx pulses) based MIMO architecture (i.e. /1/, Chapter 1) with co-located and parallel TX and RX ULAs, signal $\boldsymbol{y_i}$, (i=1,2..M_r) received by the i-th receiver antenna, and scattered by a point target with complex Reflectivity γ, and azimuth ϑ is:

$$\mathbf{y}_i = \gamma \sum_{j=1}^{M_t} a_{ij}(\theta)\mathbf{x}_j \qquad \text{i=1,2..M}_r \qquad (1)$$

with $\boldsymbol{x_1}, \boldsymbol{x_2} \ldots \boldsymbol{x_{Mt}}$ orthogonal signal *contemporary* transmitted by antennas 1-2... M_t, a_{ij} phasors accounting of delay from j-th TX element and i-th RX element.

By projection of $\boldsymbol{y_i}$ (i=1,2..M_r) on the elements $\boldsymbol{x_j}$ (j=1,2.. M_r) we recover the baseband (M_r,M_t) matrix S^{ort} with elements:

$$s_{ij}^{ort} = \mathbf{y}_i \mathbf{x}_k^T = \gamma \sum_{j=1}^{M_t} a_{ij}(\theta)\mathbf{x}_i \mathbf{x}_k^T = \gamma a_{ik}(\theta) \qquad (2)$$

This projection may be implemented in each receiver at IF level by a bank of filters matched on $\boldsymbol{x_1}, \boldsymbol{x_2} \ldots \boldsymbol{x_M}$, or at baseband level.

In practice the not perfect orthogonality of signals $\boldsymbol{y_i}$ ($i=1,2..M_r$) lead leakage between target having different azimuth ϑ. Moreover the use on only one waveform, say $\boldsymbol{x}$, transmitted cyclically in time division through all M_r antenna *TX-s*, simplify MIMO architecture and at the same time prevent any spatial leakage between TX locations. Naturally this simplification has a draw-back inherent to target radial migration from frame to frame. Supposing uniform radial speed eq. (1) is now:

$$\mathbf{y}_{ij} = \gamma a_{ij}(\vartheta) \exp(-\mathbf{j}2\pi f_d (j-1)T)\,\mathbf{x} \qquad (3)$$

with $f_d = 2v_r/\lambda$ is target Doppler frequency. Now, baseband signal matrix S has elements:

$$s_{ij} = \mathbf{y}_{ij}\mathbf{x}^T = \gamma a_{ij}(\vartheta) \exp(-\mathbf{j}2\pi f_d (j-1)T) \qquad (4)$$

Now, for filled uniform array the following relation holds:

$$a_{ij} = \exp[-j2\pi \sin(\vartheta)(\frac{i}{M_r} + j)] \qquad i=0,M_r\text{-}1 \qquad j=0,M_t\text{-}1 \qquad (5)$$

Combining eq. (4) with eq. (5), elements of s_{ij} may be expressed as:

$$s_{ij} = \gamma \exp[-\mathbf{j}2\pi(\frac{\sin(\vartheta)}{M_r} i + (\sin(\vartheta) + f_d T) j)] \qquad i=0,M_r\text{-}1;\ j=0,M_t\text{-}1 \qquad (6)$$

The phase term in eq.(6) is a bilinear form in i (RX index) and j (time index). We observe that, while coefficient of i depends only on ϑ -signal reception by different RX antennas is simultaneous-, the coefficient of j depends both on ϑ and f_d, showing leakage between azimuth and Doppler domains typical of *STAP* (*Space-Time Adaptive Processing*) context [2]. We try to break this leakage using two different techniques: *slow time processing* and TX staggering.

Slow time: TX array is scanned cyclically. So phase dependence versus time is:

$$\varphi_j = 2\pi \sin(\vartheta) \bmod(j, M_t) + 2\pi f_d T\ j \qquad j=0,1\ldots. \qquad (7)$$

with *mod* modulus operator. Sampling φ_j at $M_t T$, rather than T:

$$\varphi_k = 2\pi \sin(\vartheta) j_0 + 2\pi f_d T\ j_k \qquad j_k=j_0 + (k\text{-}1)*M_t,\ k=1,2\ldots \qquad (8)$$

phase variation received from a given TX antenna j_0 depends only on target Doppler. So spectral analysis is performed along slow time domain, while azimuth compression along TX-RX 2D domains (see **Figure 1**). The drawback of space and time domains de-leakage is to perform Doppler processing at reduced rate 1/(N*T) rather than 1/T.

TX staggering: if Tx-s antennas are activated with a pseudo-random permutation law, eq. (7) is modified into:

$$\varphi_j = 2\pi \sin(\vartheta)\, perm(\bmod(j, M_t)) + 2\pi f_d T\ j \qquad j=1,2\ldots. \qquad (9)$$

where *perm* is a random but known permutation law which is changed from on TX cycle to the next. *i.e*: for $M_t=5$, in place of the sequence (1,2,3,4,5, 1,2,3,4,5..) is transmitted the sequence *(4,1,3,2,5, 2,5,4,1,3...)*. In this way the linear behaviour of target phase versus index j (time) can be somewhere separated from the non-linear behaviour of the permutation law. We note that the same scope could be obtained with a Non Uniform Linear Array. The drawback of this technique, however, is a limitation of the Doppler azimuth scene, as will be shown later.

2. SIGNAL PROCESSING

Slow time and TX staggering processing will be described respectively in 2.1 and 2.2, and represented in **Figure 2**.

2.1 Slow time processing

The different step of processing flow, reported in Figure 2a, are now described in details. Due to TX time switching Doppler processing is done before azimuth (MIMO) processing. Range migration compensation is not necessary for narrow TX ULAs, and allows azimuth compression by 1-D FFT processing along the virtual 1-D array.

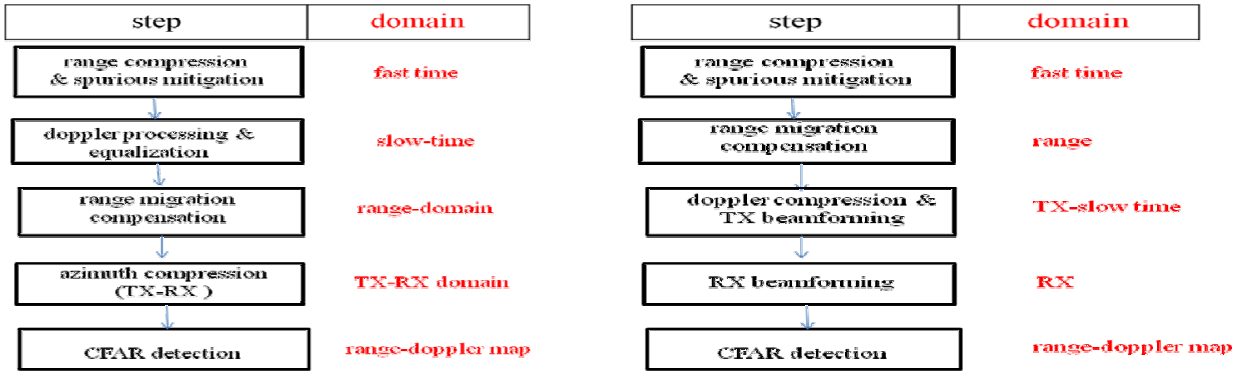

a) slow time **b) TX staggering**

Figure 2 processing flow: a): slow time , b) TX staggering

Range compression and spurious suppression

Spuriouses are originated as Inter-Modulation product of:

- the target beat frequencies with the strong direct path leakage between the Tx and the Rx
- beats among multiple real targets beats frequencies due to large RCS close targets

If not mitigated they may strongly limit radar dynamic along range domain. Spurious cancellation technique is proposed in [3].

Doppler processing

Doppler processing is performed along slow-time domain on the M_rM_t vectors of data hologram (Figure 1). Each N_r length complex vector is first processed with a double MTI (Moving Target Indicator) *(optional)* and a weighted 1-D FFT. Let h_{ijk} be the generic element of the transformed hologram, where *i,j* and *k* are respectively *RX, TX* and Doppler filter indexes. Doppler equalized elements p_{ijk} are obtained by:

$$p_{ijk} = h_{ijk} \exp(\mathbf{j}2\pi \frac{k\,j}{M_r N_d}) \qquad i=0,M_r\text{-}1; \qquad j=0,M_t\text{-}1 \qquad k=0,N_d\text{-}1 \qquad (10)$$

where N_d is number of Doppler filters ($N_d > N_r$ with zero-padded FFT-s). In eq. (10) $2\pi k/(M_r N_d)$ represents indeed the opposite of target phase change experienced between two adjacent TX-s and relative to the *k-th* filter. This phase compensation is possible only in the Fourier Transformed hologram *H*, where each Doppler filter corresponds to the peculiar Doppler term to compensate. This fact explain why in the diagram flow of Figure 2a Doppler processing is anterior to MIMO processing.

Range delay compensation

In a MIMO system 3D hologram samples are affected by different range delays because of target radial motion and of no co-located *TX and RX ULAs.* According to a consolidated rule, the larger not-compensated range delay should be less than a fraction ρ of range resolution (i.e. [2]). Target migration constrain is $\Delta_{tar}=2v_rT_o<\rho/2$, while array migration constrain is $\Delta_{TX}\approx l_{TX}\,sin(\vartheta)$, where (see Figure 3) v_r is target radial velocity, l_{TX} is TX array length, ϑ is target azimuth with respect to TX-RX array bore-sight, and $T_o=M_t\,N_r*T$ is the processed frame length. As small boat have small velocities ($|v_r|<10$ m/sec is a valid hypothesis for small boats) range delay comp. implementation depends basically from TX array length, indicatively it is necessary for $l_{TX}>$ 1 m. While intrinsically a simple operation (shift of complex envelop along range domain) it prevents azimuth beam-forming implementation by 1D FFTs.

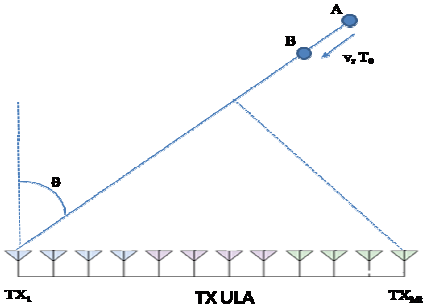

Figure 3 range delay due to target radial motion and antenna spatial distribution

Azimuth beam-forming will be described assuming or less delay compensation.

a) **No range delay compensation**.

If in the hologram P (see eq. (10)), we keep fixed a generic doppler filter k, we obtain a 2D hologram $P_k(i,j)$ $i=1.2..M_r$; $j=1.2..M_t$. Let $\boldsymbol{p}_k$ be the M_r*M_t length vector obtained by joining the columns of P_k, starting from the 1^{st} end ending with the M^{th}. $\boldsymbol{p}_k$ contains the elements of the virtual filled *ULA* with M_tM_r elements (see [1], par. 1.3). Azimuth compressed vector $\boldsymbol{v}_k$ is obtained, for each *k*, by:

$$\mathbf{v}_k = fft\,(\mathbf{w}^T\mathbf{p}_k, n_a) \qquad k=1,2..N_d \qquad (11)$$

with $\boldsymbol{w}$ weight vector and, using *MatLab* language, $fft(\boldsymbol{a},n_a)$indicates *Fast Fourier Transform* applied to vector $\boldsymbol{a}$ and zero-padded to n_a ($n_a \geq M_tM_r$). Corresponding azimuth angles (not dependent on k) are given by:

$$\vartheta_j = \arccos(1 - \frac{2j}{n_a}) - \frac{\pi}{2} \qquad j=0,1,2\ldots n_a\text{-}1 \qquad (12)$$

b) **Range delay compensation**.

Referring to eq. (12) with formal substitution of n_b in place of n_a, the set $sin(\vartheta_j),\ j=0,1,2\ldots n_b\text{-}1$, with is represented on a uniform grid of [-1,1]. It can be easily verified that if *TX* array is *range compensated* on ϑ_j, the maximum uncompensated delay over the *TX* array length l_{TX}, within the sector $(\vartheta_{j-1}, \vartheta_{j+1})$, is $2*l_{TX}/n_b$. We say that the TX array is range compensated on the generic angle *of* ϑ when the range profiles indexed by *i* (RX index), *j* (TX index), *k* (Doppler index) are range shifted by $(j\text{-}1)l \sin(\vartheta),\ j=1,2\ldots M_r$ and $l=M_r*\lambda/2$ adjacent TX element separation (see Figure 3). Then the azimuth-doppler map is reconstructed in the current angular sector, using for instance DFT evaluated to a reduced number of bins of the frequency (in this case azimuth) domain. This two-step compensation-compression procedure is repeated for each angular sector. Minimal computation charge is achieved by minimization of n_b, given the constrain:

$$2\frac{l_{TX}}{n_b} < \frac{\rho}{2} \qquad (13)$$

For instance: given $l_{TX}=20\ m$, $r=1\ m$ at least n_b=80 different azimuthal sectors are required.

CFAR processing

After azimuth beam-forming we have a 3D complex hologram V with elements v_{pkj} where $p=1,2\ldots N_s$ is range index, N_s number of range bin, $k=1,2..\ N_d$ is Doppler index, and $j=1,2\ldots n_a$ is azimuth index. If we fix a generic azimuth cell *j*, $V_k(p,j)$ represents the range Doppler map for azimuth bin *j*. Target detection are found on the range Doppler map with a *CFAR* (Constant False Alarm Rate) detector on $|V_k|$. Eventually a morphological detector of clutter may inhibit Doppler range bin from CFAR application in the case of appreciable clutter, maybe residual from MTI processing.

2.2 TX staggering processing

TX staggering processing flow is represented in **Figure 2**b. The scope is to achieve doppler processing at rate 1/T rather than $1/(M_tT)$. After *Range compression and spurious mitigation*, range migration compensation has to be performed for each angular sector (see 2.1) before *Doppler processing&TX beamforming*, in order to equalize paths from target to the different antenna TX-s. Then *RX beamforming* allows elimination of TX beamforming aliasing due to large separation of TX elements. Finally CFAR detection is performed for each azimuthal cell on range-doppler maps. Here, we limit to analyze *Doppler processing&TX beamforming*, being the peculiar step of processing chain. Moreover the whole processing flow has not been detailed because *Doppler processing&TX beamforming* suffer of dynamic limitation.

Doppler processing &TX beamforming

As shown in Figure 4, the successive *RX-TX* (M_r,M_t) 2D hologram acquired at *TX* cycles $1,2..N_r$, are merged in the time domain to form a 2D $(M_r,\ M_t*N_r)$. The k-th raw represents the signal *s* received by the *k-th* receiver during the whole frame time T_o. Signal scattered by a scenario of N_{rifl} reflectors, is:

$$s(j) = \sum_{p=1}^{N_{rifl}} A_p \exp(\mathbf{j}2\pi \frac{j\,l_p}{N_d}) \exp(\mathbf{j}2\pi \frac{perm(j)\ k_p)}{M_t}) \qquad j=1,2\ldots N_{tot} \qquad (14)$$

where $N_{tot}=M_t*N_r$ and (A_p, l_p, k_p) respectively complex amplitude, doppler index and TX beam index of the p-th scatterer, with $l_p \in (1,N_d)$, $k_p \in (1,M_t)$, $p \in (1,N_{rifl})$. In eq. (14) the phase of each point reflector is sum of a pseudo random term (*array term*) and a linear term associated to the radial target motion (*doppler term*).

The following spectral techniques have been investigated in order to estimate target Reflectivity *f(l,k.*: matched filtering, CLEAN and direct spectral estimation.

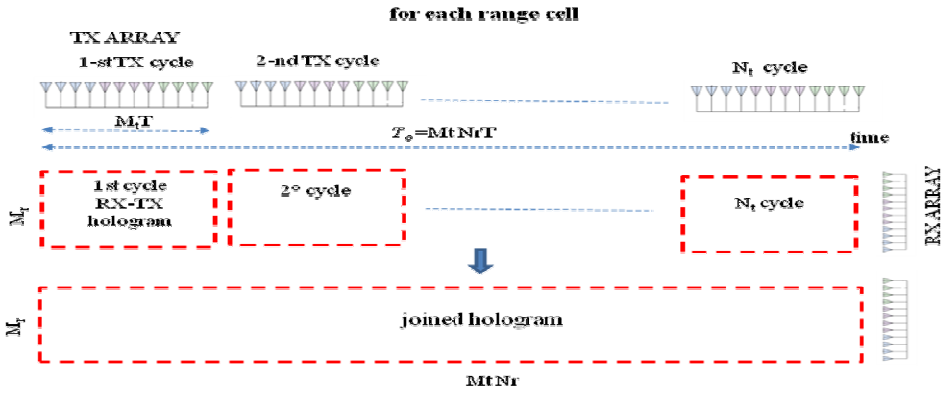

Figure 4 Combination of TX-RX hologram

a) matched filtering

Matched filter estimate $\hat{f}_{mf}$ is recovered from signal *s* as:

$$\hat{f}_{mf}(l,k)=\left|\sum_{j=1}^{Ntot} s(j)\exp(-j2\pi\frac{j\,l}{N_d})\exp(-j2\pi\frac{perm(j)\,k)}{M_t})\right| \qquad l=1,2...N_d \qquad k=1,2.M_t. \qquad (15)$$

In the case of a single scatterer (A_1,l_1,k_1) samples

$$\hat{f}_{mf}(l,k)=\sum_{j=1}^{Ntot}\exp(-j2\pi\frac{j\,(l-l_1)}{N_d})\exp(-j2\pi\frac{perm(j)\,(k-k_1)}{M_t}) \qquad (16)$$

then if $k=k_1$: $\left|\hat{f}_{mf}(l_1,k_1)\right|=N_{tot}A_1$, whereas if $k\neq k_1$ $\left|\hat{f}_{mf}(l_1,k)\right|\cong\sqrt{N_{tot}}A_1$ due to the de-coherent effect of pseudo-random $perm(j)\,(k-k_1)$ not perfectly compensated. Then the reconstructed doppler-azimuth dynamic is limited to $dyn=(N_{tot})_{dB}$. For instance *dyn=25 dB* for $N_{tot}=640$.

b) CLEAN technique

Application of CLEAN technique [4] may improve the dynamic range of the doppler- azimuth 2D map obtained at step a) by *detecting& removing* in sequence the peaks, starting from the larger to the smaller. By simulation on a three point target reflectivity 50 dB dynamic all the three reflectors have been detected.

c) direct spectral estimation

Optimum Unbiased Estimation and MMSE (Minimum Mean Square Estimation) have been tested for the direct estimation of target parameters (A_p,l_p,k_p), $p=1,N_{rifl}$ from eq. (14). Our implementations represent a 2D extensions of estimate techniques applied respectively in [6] and [7] to a 1D case.

Unfortunately at this moment we don't experience an improvement with respect to matched filtering, that is image dynamic does not improve.

2.3 Comparison of the two algorithms

TX staggering technique is more attractive because it works at rate $f_s=1/T$ rather than f_s/M_t. Unfortunately it seem to suffer dynamic limitation and application of 2D Optimum Unbiased Estimation and MMSE don't seem to overcome this problem. The reason could be that 2D spectral techniques try to recover a 2D Reflectivity distribution from a 1D hologram (see eq. 14). Moreover, CLEAN technique show to be quite sensitive to peak parameter estimation. More effort will be done do overcome this problem increasing spatial diversity through consideration of *Not Uniform Arrays*.

Moreover, the necessity to indicate a robust solution for RANGER project lead to analyze the slow time f_s/M_t solution with more detail (see Sect. 3).

3. ANALYSIS OF PERFORMANCE

In 3.1 the main MIMO parameters, essentially M_r , T and N_r , will be specified from system requirements: range $R_0=12$ *Km*, azimuth resolution $\vartheta_b<0.2°$ at boresight, processing time $T_0>100$ *msec*, and a non ambiguous interval $d_v=12.5$ *m/sec* for target radial speed. In 3.2 we show the reconstructed azimuth-Doppler map relative to a four 0 dB m^2 point scatterers target, in the hypothesis of two different radar antenna heights.

3.1 MIMO parameter specification

A basic specification for Ranger project is a filled ULA array with $M_r=M_t=20$. Assuming λ=0.1 m (S band) array width is l_{TX}=20 m. In this way azimuth beam-forming gives an azimuth resolution $\vartheta_b=1/(M_r\ M_t)=2.5*10^{-3}$ *rad* ($\approx 0.15°$) satisfying requirement ($\vartheta_b<0.2°$ at bore-sight). $d_v=12.5$ *m/sec* implies $T \le M_t \lambda/(2\,d_v) = 2*10^{-4}$ (sec), and we fix $T=200$ μ*sec*. We fix also $N_r \ge 32$, that is an integration time larger than $T_0>Mr*M_{t*}N_r$T=*128 msec*. Large coherent integration gain $g_{dB}=10*log(M_r*M_{t*}N_r)$=41 dB largely compensate for the *3dB* loss suffered within de-chirping step by the signal scattered by a target located at maximum range $R_0=12$ *Km*, which overlap with the beat chirp for only half length. Moreover $N_r \ge 32$ implies a fine radial velocity resolution $\Delta_v \le d_v/N_r$ = 0.4 m/sec. Spurious suppression technique described in [2] considers the option to re-transmit four times with each TX, instead on one, using still T as PRT, such as to give a further improvement to spurious cancellation.

3.2 Azimuth Doppler map reconstruction

Azimuth-Doppler map reconstruction is simulated on I/Q 3D complex hologram G for a given range bin in output of compression & spurious mitigation (Figure 2). A simulation reconstructs the range-doppler map implementing *Doppler processing* and *azimuth beamforming*. For simplicity range migration effects has not been considered in the generation of G. Here the main assumptions of simulation: Target model: *0 dB* m^2 *SW 0;* SNR : $\ge$ *-10 dB* on the single (range compressed) pulse at range $R_0=15$ *Km* on standard *RCS=0 dB* m^2 target. Sea Clutter model: compound clutter with an amplitude Gamma distribution and Gaussian spectrum, see [8] and [9]. Correlation coefficient versus time is modelled as: $\rho(t)=exp[-2(\pi\,\sigma_f\ t)^2]$ exp($j2\pi\,\eta_f\ t$) with $\sigma_f=2\sigma_v/\lambda$, η_f mean clutter frequency and σ_v is clutter velocity standard deviation. $\eta_f=0$ and σ_v=2 m/sec are assumed. We have assumed the improvement of GIT (Georgia Institute of Technology) Clutter Reflectivity model described in [9], Sea State=3 is assumed. Antenna target height $h_a=10$ *m* sufficient for a target distance of a rubber boat at 17Km , $h_a=50$ *m* (radar site elevated due to coast morphology constraint) Chirp bandwidth $B=100MHz$ achieving a nominal range resolution $r_y=1.5$ *m*. Vertical Polarization is assumed conservatively, being sea clutter returns larger with respect to Horizontal polarization, especially at low grazing angles. Target Reflectivity Composed of 4 point reflectors, all with Reflectivity *0 dB* m^2, radial velocity respectively [2,0.1,3,5] m/sec and azimuth [-60.2 -10.2 4.3 40.7]. Azimuth-Doppler maps have been evaluated respectively for $h_a=10$ *m* (Figure 5a) and $h_a=50$ (Figure 5b) and respectively at 4 and 6 Km from radar. In the first case sea clutter level is lower with respect to azimuth side-lobe level, practically negligible. In the second case clutter is clearly visible around null Doppler and reduce detection performance for low radial velocity target: indicatively for $|v_r| < \sigma_f$ ($\eta_f=0$).

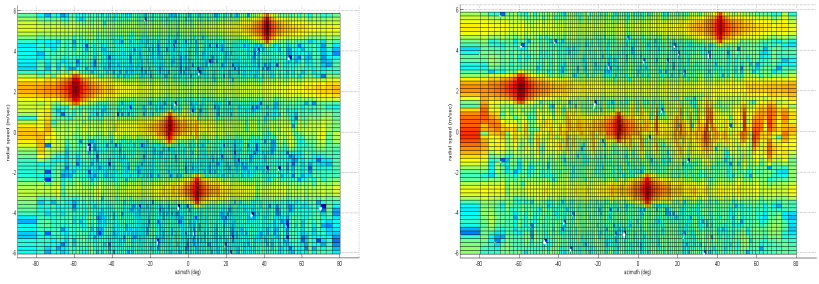

(a) *(b)*

Figure 5 Azimuth Doppler maps reconstructed Reflectivity for h_a=10 m (a) and h_a=50 m (b)

T stagger from frame to frame, with 2 PRTs around nominal PRT, may in order resolve doppler ambiguity, by extending the non ambiguous interval of radial speed from [-6.25, 6.25] m/sec to [-12.5, 12.5] m/sec, including also fast boats. In presence of large clutter ($h_a \ge 50$ m and/or sea state>5) proper selection of *T* around nominal $T=200$ μ*sec*, avoids Doppler superposition of folded target with sea clutter. Though super-clutter visibility appear realistic for the low speed point

target - and we expect a confirm by live data analysis - Doppler processing is still necessary within MIMO architecture based on *Time Domain Multiplexing* in order to separate time and space domains.

4. CONCLUSIONS

Two signal processing for a MIMO architectures based on *Time Domain Multiplexing* have been proposed in this paper: *slow time sampling* and *TX staggering*. In the first, each receiver process echoes received sequentially by the same TX element. In this way phase change do to target (doppler effect) is separated by target change due to phase change due to TX location switch. Doppler processing at a reduced rate PRF/M_t, and the necessity to detect unambiguously low speed targets (vr<6 m/sec) implies to assume a low PRT, in our case $T=200\ \mu sec$, implying an range of 12 Km largely compatible with RANGER project requirements. Due to narrow range resolution cell, narrow beam-width and slow grazing angle, due to low antenna height, a *1 m2* target is well detected in super-clutter visibility at all ranges.
The MIMO architecture shows key advantages for the detection of rubber boats with small size and reduced RCS (0dB m2) in sea Clutter: narrow range resolution cell due to large instantaneous BW, narrow beam width due to the distributed Tx antenna, and consequently the collected clutter is very small, moreover high clutter resolution due to long slow time (TM_t of 4 ms) that is useful to distinguish the target from the Clutter.
It has been simulated that the target can be detected in super clutter visibility. The low Pd typical of a CFAR detector in case of super clutter visibility is not a limitation for the radar mission of Search & Rescue; in this scenario the available time for detection can be very long (a few seconds), consequently cumulative Pd can be improved wrt single detection Pd by non-coherent integration of CFAR detections over multiple consecutive frames (T0 =128ms).
In order to reduce PRT limitation, and extend application of the same MIMO architecture to longer ranges (i.e. 50 Km), we have proposed to stagger TX element selection. The pseudo-random law of phase change results to be only partially orthogonal to the nearly linear doppler term. The effect is a limitation of azimuth-doppler map dynamic, nor application of 2D MMSE and CLEAN techniques has shown to be effective. Alternatively, in order to extend the range to 50Km , in the slow time processing architecture presented in chapter 3, the $T>700\mu sec$ must be set, consequently a non-ambiguous Doppler velocity of $d_v<3.5\ m/sec$ occurs. A T stagger frame to frame technique can overcome the Doppler ambiguity, but still it is difficult to distinguish the target from the clutter in the Range dopper maps, due to the clutter folding.
To overcome this problem, it has been estimated that, as it is for the case of 12 km range (Figure 5) also in the case of 50 km range, the detection is feasible in super clutter visibility.
This work is a part of the RANGER [4] project. RANGER has received funding from the European Union's Horizon 2020 research and innovation program under grant agreement no 700478. The authors would like to thank all partners within RANGER for their cooperation and valuable contribution.

REFERENCES

[1] J. Li, P. Stoica: *MIMO radar signal processing*, 2009 John Wiley & Sons.
[2] R. Klemm: *Principles of Space-Time Adaptive Processing,* The Institution of Engineering and Technology, 2006
[3] R. Lalli, M. Pullo, A. Manuale, A. Farina, L. Pierno, F. Prodi: *Spurious mitigation technique for TDM-MIMO FMCW radar*, 1st Maritime Situational Awareness Workshop (MSAW), Lerici, 8-10 Oct. 2019
[4] Peter W. Moo: Range-Doppler Migration in Coherent MIMO Radar, Proceedings of the 8th European Radar Conference, Manchester, 12-14 Oct. 2011
[5] Krzysztof Kulpa: *The CLEAN Type Algorithms for Radar Signal Processing* MRRS-2008, Symposium Proceedings. Kiev, Ukraine, September 22-24, 2008.
[6] T. Felhauer: *Optimum unbiased estimation, a favourable alternative to matched filter, and its suboptimum implementation by a novel mismatch filter,* IEE Radar conference, Brighton (UK), 1992.
[7] M. H. Ackroyd and F. Ghani, *Optimum Mismatched Filters for Sidelobe Suppression*, IEEE Transactions on Aerospace and Electronic Systems, Vol AES-9, No. 2, March 1973, pp 214-218.
[8] K. J. Sangston, A. Farina: *Coherent Radar Detection In Compound-Gaussian Clutter: Clairvoyant Detectors*, IEEE A&E Systems Magazine, November 2016, Tutorial, Part I of II, pp. 42-63.
[9] S. Watts, K. Wards, R. Tough: *Modelling the shape parameter of sea clutter,* 2009 International Radar Conference: *Surveillance for a Safer World***,** 12-16 Oct. 2009, Bordeaux
[10] V. G. Hansen, R. Mital: *An Improved Empirical Model for Radar Sea Clutter Reflectivity:* NRL/MR/5310-12-9346, April 2012.

*main author: francesco.prodi@leonardocompany.com; phone 0039 3289657249